An Advanced HIL Simulation Battery Model for Battery Management System Testing

Jorge Varela Barreras, Christian Fleischer, Andreas Elkjær Christensen, Maciej Swierczynski, Erik Schaltz, Søren Juhl Andreasen, and Dirk Uwe Sauer

***Abstract*—Developers and manufacturers of battery management systems (BMSs) require extensive testing of controller Hardware (HW) and Software (SW), such as analog front-end and performance of generated control code. In comparison with the tests conducted on real batteries, tests conducted on a state-of-the-art hardware-in-the-loop (HIL) simulator can be more cost and time effective, easier to reproduce, and safer beyond the normal range of operation, especially at early stages in the development process or during fault insertion. In this paper, an HIL simulation battery model is developed for purposes of BMS testing on a commercial HIL simulator. A multicell electrothermal Li-ion battery (LIB) model is integrated in a system-level simulation. Then, the LIB system model is converted to C code and run in real time with the HIL simulator. Finally, in order to demonstrate the capabilities of the setup, experimental results of BMS tests over a certain set of exemplary cases are shown.**

***Index Terms*—Battery management system (BMS), hardware-in-the-loop (HIL), lithium ion.**

I. Introduction

A well-known limitation of Li-ion batteries (LIBs) is the need for reliable electronic protection, i.e., a battery management system (BMS), to avoid electric or thermal abuse. The reason for this is to minimize battery degradation and to prevent thermal instability, conditions that can lead certain chemistries to a thermal runaway. Moreover, in order to maximize battery capacity, active or passive balancing circuits are implemented in BMSs. Without balancing, if multiple cells are connected in series, the weakest cell constrains the entire pack performance. Local operational differences and uncertainties at the material level are related to these cell-to-cell variations, which lead to further differences in the cell-to-cell performance over time. But an advanced BMS does not only balance and keep the battery within a certain safe operating area (SOA), it may also manage a heating/cooling system, run fault tolerance routines, control the charging process, or provide a diagnosis of battery states such as power capability, state-of-charge (SOC), state-of-health (SOH), or remaining run-time. Fig. 1 provides a high-level representation of a real battery system, from the perspective of typical BMS functions and interfaces [1]–[16].

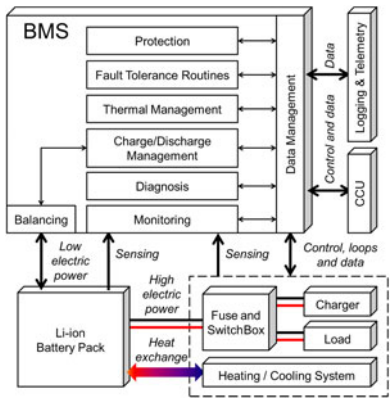

Fig. 1. Overview of typical BMS functions and interfaces.

Nevertheless, since electrochemical batteries are not ideal devices and limited sensing and actuation is possible, these BMS tasks are not trivial. Voltage, current, and cell surface temperatures are the only measurable variables and may be related to the battery states through highly nonlinear functions [17]–[19]. Due to aforementioned issues, it is easy to understand the interest in study of BMSs, especially for applications with high management requirements, like e-mobility. This means that developers and manufacturers of sophisticated BMSs may require extensive testing of controller hardware (HW) and software (SW), such as analog front-end (AFE) and the performance of generated control code. In comparison with tests conducted on real batteries, tests conducted on a hardware-in-the-loop (HIL) simulator may be more cost and time effective, easier to reproduce, and safer beyond the normal range of operation, especially at early stages in the development process or during fault simulation (see Fig. 2).

However, as discussed in the following section, it is not easy to provide an HIL simulator environment able to provide in real-time signals for testing a wide variety of BMS functions, such as cell protection; safety validation measuring of current, voltage, and temperature; balancing of cells; analysis and parameter prediction; fault tolerance through fault insertion testing; logging, telemetry, and external communications (see Figs. 1 and 2).

In this paper, an advanced HIL simulation battery model with state-of-the-art capabilities is developed for the purposes

Manuscript received September 2, 2015; revised January 29, 2016 and April 27, 2016; accepted May 24, 2016. Date of publication June 29, 2016; date of current version November 18, 2016. Paper 2015-TSC-0678.R2, presented at the 2015 Tenth International Conference on Ecological Vehicles and Renewable Energies, Monte-Carlo, Monaco, Mar. 31–Apr. 2, and approved for publication in the IEEE Transactions on Industry Applications by the Transportation Systems Committee of the IEEE Industry Applications Society.

J. V. Barreras, M. Swierczynski, E. Schaltz, and S. J. Andreasen are with the Aalborg University, Aalborg 9000, Denmark (e-mail: jvb@et.aau.dk; mas@et.aau.dk; esc@et.aau.dk; sja@et.aau.dk).

C. Fleischer and D. U. Sauer are with the Institute of Power Electronics and Electrical Drives, Rheinisch-Westfälische Technische Hochschule (RWTH) Aachen University, Aachen 52062, Germany (e-mail: Christian.Fleischer@isea.rwth-aachen.de; sr@isea.rwth-aachen.de).

A. E. Christensen is with the Lithium Balance A/S, Ishoj 2635, Denmark (e-mail: andreas@lithiumbalance.com).

Color versions of one or more of the figures in this paper are available online at http://ieeexplore.ieee.org.

Digital Object Identifier 10.1109/TIA.2016.2585539

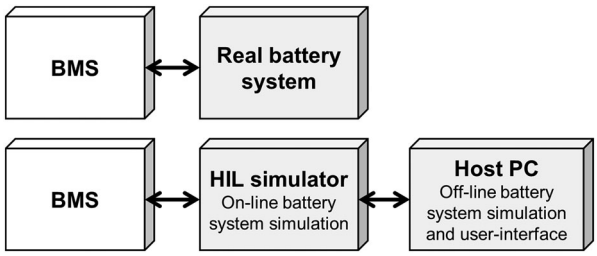

Fig. 2. BMS testing: real battery system versus HIL simulation concept.

of BMS functional testing and fault insertion on a commercial HIL simulator. The HIL simulator running the developed battery model is able to provide signals for testing any BMS function, such as monitoring, protection, balancing, control of the current path, heating/cooling management, diagnosis or data management, in the frame of fault insertion and functional testing. The HIL simulation battery model is based on LIB models, which are integrated in a system-level simulation with real-time interface (RTI) capabilities with the commercial HIL simulator setup. Then, the HIL simulation battery model is converted to C code and emulated in real time with the HIL simulator (see Fig. 2). Finally, in order to show the capability of the HIL simulator, a commercial BMS is tested through a wide variety of exemplary cases in an e-mobility application.

As aforementioned, the HIL simulation battery model consists not only of the LIB model, but also of certain model management controllers and other models of typical components of an LIB system as shown in Section III. The model management controllers are used to configure the HIL simulation battery model for different test cases. Typical components of an LIB system considered in the simulation include the temperature and current sensors, the switch box, the charger or the load, which is modeled based on a conventional dynamic model of a battery electric vehicle. With regard to the LIB model, an advanced electrothermal multicell equivalent circuit model (ECM) coupled with an aging model is proposed. It is worth noting that the aging model presented is not used for any purposes other than generating realistic cell-to-cell parameter variations. In this way, different realistic testing scenarios may be reproduced. This approach, to the best of our knowledge, is a novelty in the literature.

The paper is organized as follows. In Section II, the concept of battery emulation is reviewed based on the literature. In Section III, the developed HIL simulation battery model is presented, with focus on the LIB system. The electrothermal multicell ECM coupled with an aging model is described and its parameterization is detailed, based on experimental data from large format 40 Ah Li-ion pouch cells with nickel manganese cobalt oxide (NMC) cathode manufactured by Kokam. Models of other typical components of the battery system are also outlined in this section. In Section IV, the experimental setup for HIL simulation is presented, distinguishing between the commercial BMS under test and the HIL simulator itself. In Section V, experimental results of the interaction of the BMS with the real-time simulator are provided. Finally, Section VI gives the conclusion.

II. Critical Review of Battery Emulation

Nowadays HIL simulators are widely employed to prototype, design and test complex real-time systems in many applications due to a combination of safety, feasibility, time- and cost-effectiveness factors. In the next section, the HIL simulation approaches in relation with LIBs presented in scientific and technical literatures are reviewed with a special focus on automotive applications.

HIL simulation uses some virtual or emulated components and some physical components. If a real LIB system is used, the method is so-called battery-in-the-loop (BIL) or battery-HIL. BIL simulation is proposed in automotive applications for the purposes of battery evaluation [20], BMS validation [1], verification of battery models [21], or assessment of power or energy management strategies [2], [22], [23], considering a complete virtual vehicle [1], [2], [20], [21] or in combination with other real components [22], [23].

HIL simulation methods with virtual LIBs, pack-based (or aggregated) approaches [3], [24]–[38] are more frequent in literature than cell-based (or multi-cell) approaches [4]–[13]. In general, in order to control the charging/discharging process, any BMS for a series or series–parallel-connected battery pack should at least monitor the pack voltage, the pack current, the single cell voltages and the temperatures at cell or pack level. Moreover, cell balancing is required to avoid severe SOC unbalances over time due to cell-to-cell differences [14], [16], [39]. Hence, it is easy to understand that, for purposes of complete BMS validation, cell-based HIL simulation is preferred over pack-based.

HIL simulation using virtual LIB pack-based methods is proposed in stationary [36]–[38] and automotive applications [3], [24]–[35], the latter with the goal of electric powertrain evaluation [24]–[28], BMS validation [3], [29], vehicle controller unit testing [30], assessment of power or energy management strategies [31], [32] or verification of the feasibility of the HIL concept [33], [34]. On the other hand, HIL simulation using virtual LIB cell-based methods is proposed either for addressing BMS validation [4]–[12] or only testing balancing circuits [13].

If there is high power flow between real components and the HIL simulator, the technique is called power-HIL (PHIL) [24]–[28], [31], [32], [34]–[36]. This a common feature of pack-based HIL simulators used for electric powertrain evaluation [24]–[28]. PHIL simulation is also applied in [35] to lead-acid technology, where a portable system using virtual 12 V SLI battery is presented and tested during motor cranking in a car.

In contrast, the usual case in HIL simulation only involves a low level of power, voltage, and current related with analog and digital I/O signals or communication networks, e.g., Controller Area Network (CAN) bus [1]–[13], [20]–[23], [29], [30], [33], [37], [38]. In general, this is the case of all the cell-based HIL simulation approaches found in the literature [4]–[13]. In some cases, a strictly communication-based approach is proposed [4]–[6], [10], [30], [37], [38], which means that BMS functions such as measuring or balancing cannot be tested, either at cell or pack level.

Regarding balancing, an isolated power interface for each cell in series (or group of cells in parallel in case of a

series–parallel-connected pack) is desired to exchange bidirectional power flow between virtual cells and real electric circuits. But such interface is only presented in cell-based simulators described in [11]–[13]. Results are shown, respectively, for only 1, 4, or 6 cells in series, and current levels at 200 mA, 1.45 A, or 5 A. Moreover, it should be noted that the setup presented in [13] is only targeted for testing balancing circuits, and not for testing any other BMS functions.

With regards to the temperature emulation, it is claimed in several references, but the thermal model is either not described [3], [4], [7], [29], [33] or the temperature is artificially introduced [5]. In fact, a thermal model is only presented in [34]. However, a pack-based approach is followed and the lumped ECM described is parameterized without experimental data. Moreover, the self-made HIL simulator setup presented can only run discharging profiles.

The most common approach for battery modeling methods is electrical models based on ECMs, e.g., impedance-based modeling (abstract approach) [3], [6], [7], [11]–[13], [21], [24]–[29], [32], [34]–[37]. Other approaches are proposed rarely in the literature. ECMs can provide information about the macroscopic quantities that are monitored by a BMS, i.e., current, voltage, and temperature (if a thermal model is included), offering a better tradeoff between complexity and accuracy than other mathematical or physic-chemical approaches, like the ones proposed in [24] and [31]. In [24], an extended modified Shepherd model (abstract approach) is proposed, and in [31], a dual-foil-based model (physic-chemical approach).

However, ECMs do not allow extrapolation from one material or cell designs to another one. Therefore, for a universal BMS validation, a library of battery models for different cell sizes, formats, chemistries, and manufacturers are desired. Such a library is not presented in the reviewed literature.

Moreover, the accuracy of the ECM lays on the circuit topology and the component dependencies on SOC, SOH, current, or temperature. The common approach is to use nonlinear dynamic ECMs with two RC elements. This circuit topology may account for most important dynamic effects. However, simple or no dependencies are usually considered in the literature. For example, only SOC dependencies in open circuit voltage are considered in [6], [12], [25], [27], [36], [37] and the dependencies are not considered or are not well defined in [3]–[5], [26], [28], [33], and [34].

It should be noted that even if a nonlinear dynamic ECM with two RC elements is used, the model may not reproduce accurately realistic battery profiles if only a few or nondependencies are considered in the circuit components, as discussed thoroughly in the literature related to battery modeling [17]–[19], [40]–[43].

Furthermore, in order to account for cell-to-cell differences or emulating different testing scenarios, an aging model can be coupled to the electrical model. This approach is followed in this paper and to the best of our knowledge is a novelty in the literature. However, it is worth noting that aging prediction models are out of the scope of this paper. With rising interest of BMS's applications, like e-mobility and Smart Grid, these complex functionalities have become increasingly important

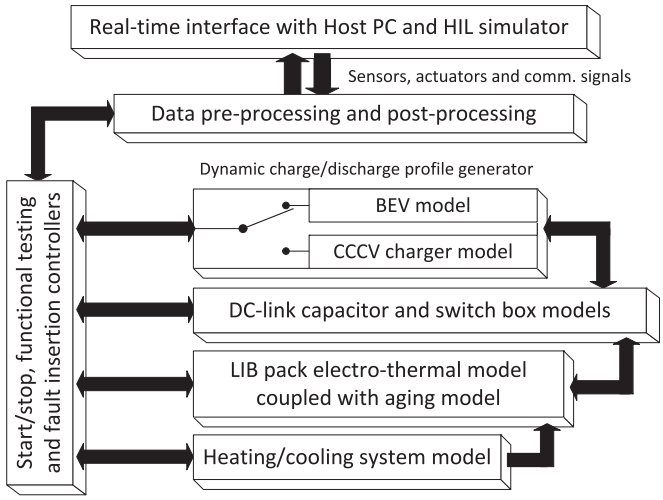

Fig. 3. Overview of the HIL simulation battery model.

[15], [39]. Similarly, testing of control strategies for balancing systems can be performed using an HIL simulator equipped with a communication interface, e.g., CAN-based. However, a complete analysis and validation of balancing system SW and HW can only be achieved if the HIL simulator setup can provide isolated power interfaces for each cell (or group of cells in parallel) in series. Taking into account the considerable attention that balancing systems have enjoyed in the literature since the introduction of LIBs [16], [44]–[46], it is easy to understand the importance of this advanced feature.

As a rule of thumb, it can be stated that, for purposes of general functional analysis of a BMS, simpler battery models may be used. However, more accurate models may be implemented with the aim of ensuring that complex functionalities of a BMS, such as diagnostic algorithms for SOC, state-of-function or SOH estimation, can be analyzed and validated using HIL simulation.

III. HIL SIMULATION BATTERY MODEL

In this section, the HIL simulation battery model is presented, with special focus on the LIB system model. As aforementioned, the HIL simulation battery model consists not only of the electrothermal multicell ECM coupled with an aging model, but also of the simulation model management controllers and other models of typical components of a battery system, like the temperature and current sensors, the switch box, the charger, or the load as shown in Fig. 3.

In Sections III-A-E, the design and characterization of the LIB electrothermal multicell ECM coupled with an aging model is presented. Parameterization is based on a commercial 40-Ah high-energy Kokam SLPB100216216H pouch cell. The ECM model consists of an inductance, an ohmic resistor, and two ZARC elements in series. Experimental pulse power characterization, capacity check, electrochemical impedance spectroscopy (EIS), and anisotropic thermal diffusivity measurement techniques are used for parameter estimation, taking into account aging, temperature, and SOC dependencies. Results are presented for a Kokam cell for illustrative purposes, but a full library has been developed including battery cells with

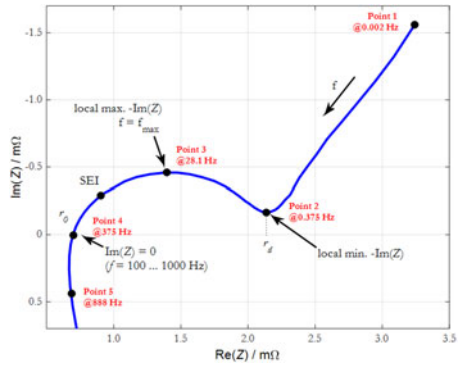

Fig. 4. Nyquist plot of the complex impedance of a Kokam 40-Ah NMC-cathode cell.

different formats (cylindrical, pouch, prismatic), capacities (2, 40, 53, 100 Ah) and cathode chemistries [NMC, Lithium Titanate Oxide (LTO), Lithium Iron Phosphate (LFP)], including other manufacturers such as Sanyo, Panasonic, or SkyEnergy. In Section III-F, the temperature sensors model is outlined. Finally, in Section III-G, the fuse and switch box model is presented, taking into account all the components.

A. Impedance Spectrum Analysis

In Fig. 4, EIS measurements conducted on the Kokam 40-Ah NMC-cathode cell are presented in a Nyquist plot. At high frequencies (>0.8 kHz), the cell shows inductive behavior caused by inductive reactance of metallic elements in the cell and wires. This is modeled as an inductor in series in the ECM. At a frequency of 375 Hz, pure resistive behavior is observed, related with the sum of the ohmic resistances of current collectors, active material, electrolyte, and separator. This effect is modeled as a resistor in the ECM. At lower frequencies, one depressed semicircle is observed in the spectrum. This is associated to an Solid Electrolyte Interphase (SEI) effect superimposed with the double layer capacity and the charge-transfer resistance at the electrodes. All these effects can be modeled by using a ZARC element in the ECM. At frequencies below 0.375 Hz, a linear slope with an angle of 45° is observed. This is associated with the diffusion process and can be also approximated by another ZARC element.

A ZARC element is made up of a resistor in parallel with a constant-phase-element (CPE):

$$\omega_0 = \left(\frac{1}{A \cdot R}\right)^{\frac{1}{\xi}} \Longleftrightarrow \underline{Z} = A \cdot (j\omega)^{-\xi} \tag{1}$$

$$\omega_{0,\mathrm{ZARC}} = \omega_{0,\mathrm{RC}} = \frac{1}{C_{\mathrm{RC}} \cdot R} \tag{2}$$

$$\Longleftrightarrow C_{\mathrm{RC}} = \frac{1}{\omega_{0,\mathrm{RC}} \cdot R}. \tag{3}$$

A CPE consists of a generalized capacity and depression factor. If the depression factor is equal to 1, the ZARC element corresponds to a simple RC element. If it is equal to 0, it just represents a resistor in series.

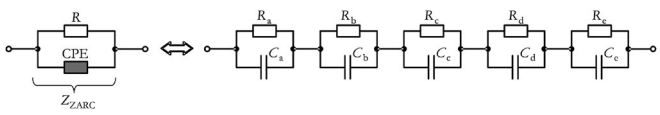

Fig. 5. Approximation of ZARC element through series connection of RC elements [34].

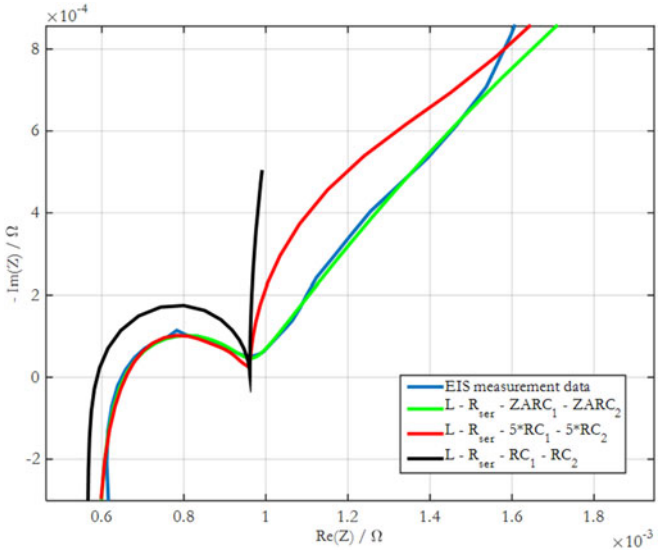

Fig. 6. Comparison of different model approximations.

B. Approximation of ZARC Elements

ZARC elements are able to accurately reproduce the impedance spectra of LIBs, but it is impossible to transfer without approximations their parameters from the frequency domain into the time domain. A common method to approximate ZARC elements is using a variable number of RC-elements (see Fig. 5). Each of the individual RC elements represents a semicircle in the Nyquist plot. To represent the ZARC exactly, infinite RC elements are needed. Nevertheless, taking into account the computational cost versus accuracy, a few RC elements are sufficient for a good approximation.

As observed in Fig. 6, the error for five RC elements in comparison to the approximation with only one RC element is reduced to a satisfactory result. The overall approximation equation is derived as follows [17]:

$$Z_{2\mathrm{ZARC}}(j\omega) = R_{\mathrm{ser}} + \frac{R_1}{1 + (j\omega)^{-\xi} \cdot R_1 \cdot C_1} + \frac{R_2}{1 + (j\omega)^{-\xi} \cdot R_2 \cdot C_2}. \tag{4}$$

C. ECM Parameter Identification

Some parameters of the ECM can be directly derived from the impedance spectrum. For example, the series resistance at high frequencies can be estimated from the intersection of the spectrum with the real part axis. Other parameters, like the inductor in series, can be neglected in some cases [18], for

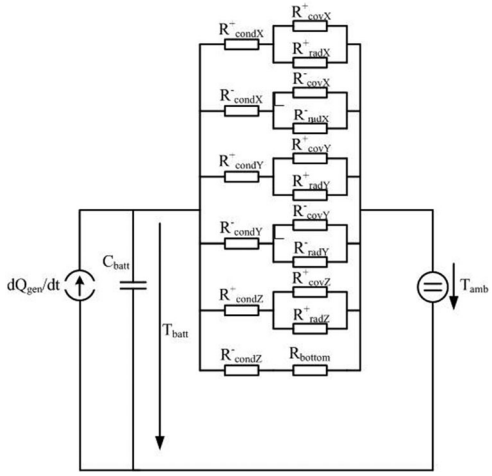

Fig. 7. Employed equivalent circuit for thermal modeling.

example, if electric vehicle applications are simulated, due to their characteristic slow dynamics. Moreover, it does not make sense to simulate phenomena that cannot be measured due to limited sampling rate of the BMS or the HIL simulator.

An in-house tool based on MATLAB Easyfit function is applied to fit the experimental EIS data in order to parameterize the ECM. The Nelder–Mead simplex search algorithm is used, which allows an accurate and precise emulation of the impedance spectra based on the modeling function. This function is crucial, because it defines the quality and robustness of the parameter identification process. It should be noted that it is always useful to define starting parameters derived directly from the impedance spectrum [19].

D. Thermal Model

Thermal effects modeled at the cell level using an ECM are illustrated in Fig. 7. The underlying processes such as heat flow dQ/dt or temperature are converted to current and voltage. Therefore, radiation, convection, and heat conduction are represented by a voltage drop over nonlinear thermal heat transfer resistances as

$$R_{\text{radiation}} = T_1 - T_2/(A \cdot \alpha_{1,2} \cdot (T_1^4 - T_2^4)) \tag{5}$$

$$R_{\text{convection}} = 1/A \cdot \alpha \tag{6}$$

$$R_{\text{conduction}} = d/\lambda \cdot A \tag{7}$$

with d representing the thickness, λ the specific heat conductivity, and α the convection coefficient.

The temperature of a volume element is calculated using the current temperature and its change. The temperature of an element is increased by the temperature difference $\triangle T$, once a heat $\triangle Q$ is applied. The heat is proportional to $\triangle T$:

$$\triangle Q = C \cdot \triangle T. \tag{8}$$

C represents the heat capacity of the element and depends on the material and mass. $\triangle T$ is calculated by

$$\frac{dT}{dt} = \frac{1}{C}\left(\frac{dQ_{\text{received}}}{dt} - \frac{dQ_{\text{delivered}}}{dt}\right). \tag{9}$$

TABLE I
THERMAL PARAMETERS EXTRACTED BY ANISOTROPIC THERMAL DIFFUSIVITY MEASUREMENT

Heat conductivity in-plane	33	W/(m · K)
Heat conductivity through-plane	0.61	W/(m · K)
Density	1.982	kg/(dm^3)
Heat capacity	860	J/(kg · K)
Mass	1.18	kg

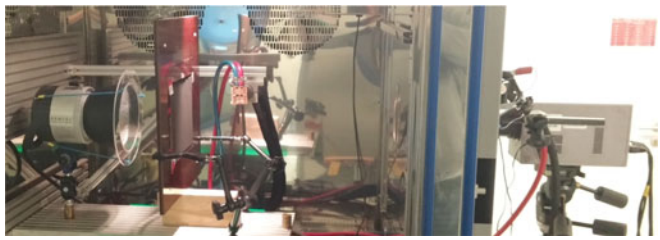

Fig. 8. Active thermography test bench.

At battery pack level the following heat transfer phenomena are considered:

1) transfer within a cell (mostly heat conduction);
2) transfer to the environment (convection and radiation);
3) transfer to neighboring cells (heat conduction, similar to a.).

The heat conductivity is defined by

$$\frac{dT}{dt} = \frac{1}{C} \cdot \sum(-T - T_i/R_i) \tag{10}$$

with index *i* describing the thermal resistance R_i and conductivity of the neighbors. The heat exchange with the environment is based mainly on the convection and radiation and described as

$$\frac{dT}{dt} = \frac{1}{C} \cdot \sum\left(\frac{-dQ_{\text{conv}}}{dt} - \frac{dQ_{\text{rad}}}{dt}\right) \tag{11}$$

with

$$\frac{dQ_{\text{conv}}}{dt} = \alpha_{\text{con}} \cdot A \cdot (T - T_i) \tag{12}$$

$$\frac{dQ_{\text{rad}}}{dt} = \alpha_{\text{con}} \cdot A \cdot (T^4 - T_i^4). \tag{13}$$

The thermal parameters presented in Table I were determined by nondestructive experimental tests. The heat capacity was just calculated from cooling curves under controlled ambient temperatures. With regard to thermal conductivity, it was calculated from the product of cells density, specific heat capacity, and thermal diffusivity as described in the American Society for Testing and Materials (ASTM) standards. The tests were conducted on a self-made active thermography test bench (see Fig. 8). Its design, measurement principle and data analysis methods were directly based on laser flash method, but using different heat power sources, following ASTM standards.

A flash lamp method was used for calculation of in-plane thermal diffusivity from temperature variation measurements. After exciting the front plane of the cell uniformly with a flash lamp, the rise of temperature over time in the rear face plane was

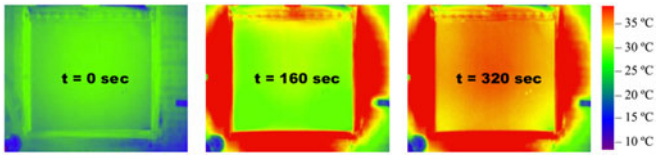

Fig. 9. Thermograms from in-plane thermal diffusivity measurements.

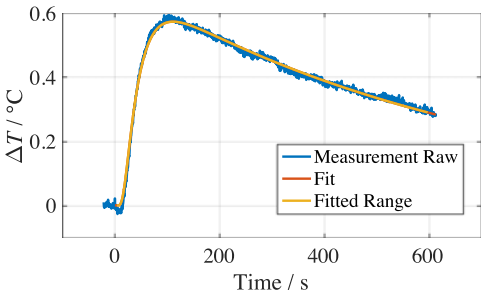

Fig. 10. Thermal diffusivity: experimental results versus model fitting.

recorded by a commercial thermal imaging camera provided by Thermosensorik (see Fig. 9).

A special fixture was designed to keep the pouch cell stable during the tests. The frame consisted of electrically and thermally insulated Pertinax base plates blanked out in the exact dimensions of the cell. Then the cell was clamped between two plates. Any gaps between the cell and the base plates were covered with thermally insulated tape in order to prevent unwanted transmission of infrared radiation to the opposite side of the cell. The battery cell surface was cleaned and sprayed with graphite for uniformly distributing the flash light energy over the entire surface. On the other hand, a liquid-cooled single-winded induction coil supplied by a high-frequency generator was used as heat power source for through-plane measurements. Due to the cell surface-to-thickness ratio, based on the laboratory experience, an induction coil placed close to the cell tabs is preferred over the flash lamp for through-plane experiments on LIB pouch cells. Thermal diffusivity was finally obtained from fitting the whole experimental data using an in-house tool based on MATLAB (see Fig. 10). It is worth noting that in this paper heat generation due to entropic or phase change, changes in the heat capacity and mixing have all been neglected. With regard to the contribution of reversible or entropic heat, it should be noted that it is neglected in many studies when the focus is not in battery performance at low C-rates. Regarding the heat generation due to phase change, changes in the heat capacity and mixing, they are commonly neglected [14], [40], [47], [48].

E. Aging Model for HIL Simulation

In order to emulate the variation of cell-to-cell characteristics, the impedance-based ECM is coupled to an aging model. This model maps the results of the parameterization from accelerated aging tests of battery cells cycled with a real driving cycle. A physical-based function is extracted from the experimental data in order to describe the aging state of the cell. All the cycling tests were carried out at different temperatures based on the average yearly temperatures of Germany. The increase of

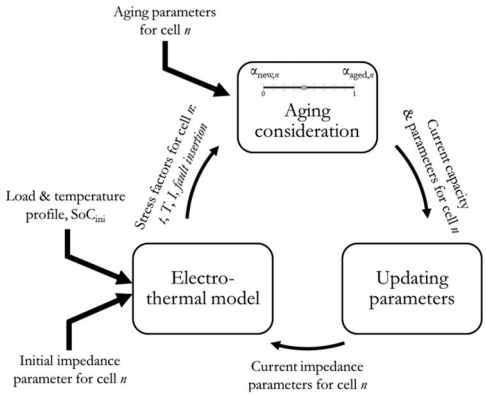

Fig. 11. Online integration of individual cell aging simulation with electrothermal model.

internal resistance and loss of capacity are monitored every 100 driving cycles conducting checkup or reference performance tests.

The checkup tests consist of a pulse power characterization test for current dependence investigation and a capacity check. The pulse power characterization test is intended to determine the internal resistance over the cells usable voltage range using a test profile that includes both discharge and charge/regen pulses. The test profile is applied to the cell under test for different temperatures in consecutive steps of 10% SOC. The SOC is adjusted based on the accumulated Ah referring to the nominal capacity. The resistance is calculated as the difference between the voltage before the discharge pulse and Δt after the beginning of the discharge pulse, divided by the amplitude of the current. The capacity check tests consist of a typical CCCV charge and CC discharge cycle conducted at 1 C-rate and different temperatures. It should be noted that during the checkup tests the cells are operated always inside an SOA limited by certain temperatures, voltages, and currents specified in the manufacturer's data sheet.

Finally, the ZARC element parameters are identified based on EIS measurements. The impedance spectra are also measured at different SOC and temperatures for using frequencies between 10 mHz and 5 kHz.

To represent the individual aging states of the cells, three parts are integrated as shown in Fig. 11:

1) impedance-based electric model;
2) thermal model;
3) aging simulation.

Every aging parameter was extracted separately and can be changed offline or on-the-fly while running an HIL simulation. Hence, it is possible to represent realistic operating conditions of multicell battery packs by applying a statistical distribution of the individual aging states. Therefore, using the three part LIB model proposed here, a full range of realistic scenarios can be addressed at the LIB battery system-level HIL simulation.

F. Temperature Sensor Model

A BMS may monitor temperature sensors throughout the whole battery system, although battery systems may differ in

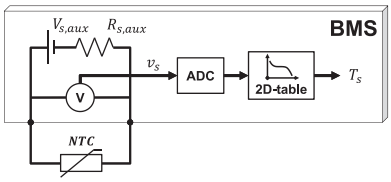

Fig. 12. Abstraction of an NTC thermistor-based temperature measurement of a BMS.

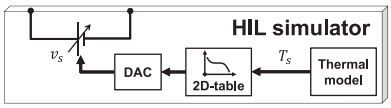

Fig. 13. Abstraction of HIL simulation setup for an NTC thermistor.

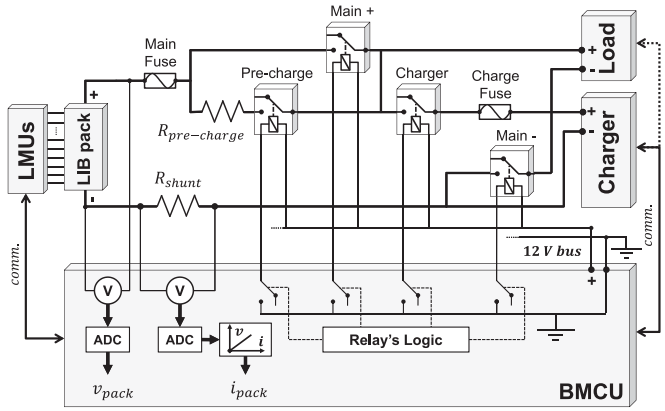

Fig. 14. Schematic of exemplary fuse and switch box topology and its interfaces.

the number, location, and type of devices used to measure the temperature. The commercial BMS under test in this paper uses negative temperature coefficient (NTC) thermistors. One temperature sensor per cell, located in a central position, is assumed for emulation purposes. NTC thermistors are thermally sensitive semiconductor resistors that exhibit a nonlinear decrease in effective resistance as temperature increases. This electrothermal behavior can be modeled analytically, by means of the SteinhartHart equation [49], [50]. In practice, NTC thermistors are usually characterized in manufacturers datasheets by a B parameter, which appears in the so-called B parameter equation. The B parameter equation presented in the following is derived from the well-known Steinhart–Hart equation using a certain change of variables:

$$\frac{1}{T_s} = \frac{1}{T_{s,0}} + \frac{1}{B} \ln\left(\frac{R_s}{R_{s,0}}\right) \tag{14}$$

where all the temperatures are in Kelvin and all the resistances in Ohm, with T_s representing the current semiconductor sensing device absolute temperature, R_s the current resistance, and $R_{s,0}$ the device resistance at temperature $T_{s,0} = 25$ °C. Solving for R_s results in

$$R_s = R_{s,0}\, e^{-B\left(\frac{1}{T_{s,0}} - \frac{1}{T_s}\right)}. \tag{15}$$

Knowing the characteristics of the sensor, represented by B, $R_{s,0}$, and $T_{s,0}$, and the parameters of the sensor excitation circuit, represented by $V_{s,\text{aux}}$ and $R_{s,\text{aux}}$, T_s may be estimated analytically in the BMS from a simple measure of the NTC thermistor voltage v_s. Another approach, illustrated in Fig. 12, is to generate and implement a NTC temperature-voltage look-up table. Based on the previous, a resistorless emulation of an NTC thermistor is possible by means of a controlled voltage source, as sketched in Fig. 13. A dedicated analog output board of the HIL simulator is used in this paper for this purpose.

G. Fuse and Switch Box Model

Due to safety issues, LIB systems include installation of dc circuit breakers in the current path. In high-voltage LIB packs, used, e.g., in e-mobility applications, fuses and relays are commonly integrated in a so-called fuse and switch box. Moreover, the system may require: a precharge circuit, for energizing the dc-link capacitor; a current measurement device, for instance, a shunt resistor or a hall effect sensor; and external communication with a BMS, which may control the relays and measure the pack voltage and current. The design of the fuse and switch box, particularly the device selection and location, may differ widely depending on the specific characteristics of the LIB system and its application.

For illustrative purposes, an exemplary topology of a fuse and switch box and its interfaces is shown in Fig. 14. This fuse and switch box is made up of four relays and two fuses, a precharge resistor $R_{\text{precharge}}$ and a shunt resistor R_{shunt}. Note that a BMS with a master–slave topology is represented, since it is the case of the commercial BMS tested in this paper, as explained in the next section. The relays allow the system to operate in three modes: stand-by or idle, discharge, and charge. Furthermore, it should be noted that, since the dc-link may be connected to a capacitive load at the load or the charger side, i.e., a dc-link capacitor, inrush currents have to be limited whenever the operating mode changes from stand-by to charge or discharge. For this purpose, a precharge circuit, which may consist of a precharge resistor in series with a precharge relay, could be implemented (see Fig. 14). The BMS is behind all the relays logic and controllers. In the HIL simulator presented in this paper, both the relays control signals and LIB pack voltage v_{pack} signals (see Fig. 14) are transmitted from/to the BMS via CAN communication. Fuses are not considered, but a complex fuse model may be included in future extension of this work. Regarding the relays, they are represented as ideal switches in series with a static resistor. The precharge resistor $R_{\text{precharge}}$ (see Fig. 14) is rated according to a desired precharging time of 1 s, taking into account the system nominal voltage, the dc link capacity and the power dissipation.

On the other hand, the BMS is configured assuming that a shunt resistor R_{shunt} is used for pack current i_{pack} measurement using analog circuitry (see Fig. 14). By using Ohm's law, a simple resistorless emulation is possible by means of a controlled voltage source. Since a dual voltage analog output is not available in the HIL simulator setup, an external single-to-dual

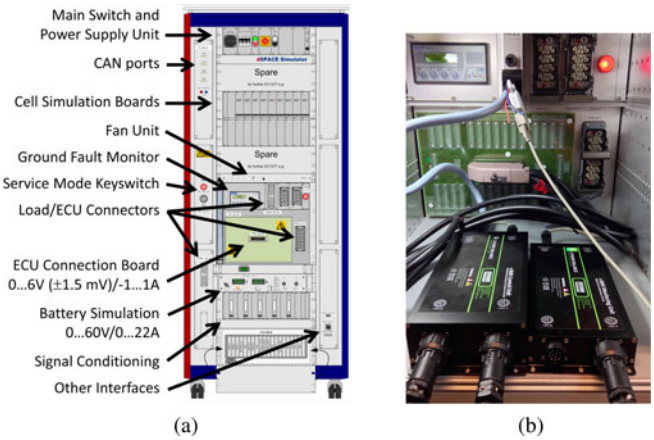

Fig. 15. Setup of hardware-in-the-loop test bench.

voltage conversion board is implemented. Note that the polarity of the shunt voltage drop depends on the direction of the LIB pack current.

IV. Experimental Setup for HIL Simulation

A. Commercial BMS Under Test

The commercial BMS under test is the sBMS v6 provided by Lithium Balance A/S (see Figs. 15 and 16). The BMS uses a master–slave configuration, where each slave unit can be configured to supervise eight cells and two temperatures. The slave, so-called local monitoring unit, is capable of passive balancing with up to 1 A simultaneously on all eight cells and will automatically reduce the balancing power if the heat cannot be dissipated at high enough rates. Four slave units are used in the experiments presented in this paper. However, a total of 32 slave units can be used for each master, giving a total of 256 supervised cells and 64 temperature inputs. The master, the so-called battery management central unit, is capable of measuring LIB pack current, LIB pack voltage, isolation faults, and contactor faults. Communication to external systems is provided through a configurable CAN bus interface, where any parameter can be broadcasted. The control of contactors, switches, and fans are all implemented in the BMS and can have a multitude of configurations.

B. HIL Simulator

The commercial HIL simulator test bench is provided by dSPACE GmbH (see Fig. 15) and interfaces with the BMS under test and a host PC either via electrical, optical, or CAN bus interfaces (see Fig. 16). It is a very complex modular system built according to customer-specific requirements. It consists of multiple racks and integrates many off-the-shelf components like digital signal processors (DSP), I/O cards, cell voltage emulation boards, power supplies, or signal conditioning boards.

The voltage emulation at the cell level is performed with several EV1077 battery cell voltage emulation boards. Each of these controllable buffer amplifier boards can emulate four cells and be configured in order to match specific test requirements. It can provide a continuously controllable voltage in a range of 0–6 V 1.5 mV for each of the outputs. This relatively wide voltage range allows not only emulation of both overvoltage and under voltage scenarios, but also emulation of short circuit faults between cells. Furthermore, broken wire faults could be also reproduced by controlling a series of switches placed in an interface board between the connection board and the EV1077 boards.

The EV1077 voltage outputs are galvanically isolated, allowing series connection. In the experiments presented in this paper 8 EV1077 boards are used to emulate 32 cells in series, but the setup could be extended with up to 24 EV1077 boards in order to allow emulation of 128 cells (or group of cells in parallel) in series. Regarding the dynamic response, any voltage reference value step can be followed in less than 500 s. This feature combined with high computational power of the DSP and a fast data transmission enables a maximum update rate for all the cell's voltages of 1 kHz. Furthermore, a bidirectional balancing current of maximum 1 A is allowed, which enables testing of both active and passive cell balancing systems. A number of other I/O cards are used to provide communication interfaces (e.g., CAN Bus) or emulation of temperature sensing or battery pack current sensing-based continuously controllable voltage outputs.

The LIB system simulation model, illustrated in Fig. 16, is developed offline on MATLAB/Simulink SW from Mathworks. An implementation SW provided by dSPACE, the so-called RTI, provides blocks that link the I/O capabilities of the dSPACE HIL simulator to the MATLAB/Simulink models. Furthermore, RTI extends the functionalities of the MATLAB/Simulink C code generator, enabling automatic generation of the C code from the offline LIB system model. Once compiled, this code is ready to be downloaded to the dSPACE HIL simulator HW from a host PC, which is connected to the real-time HW via a link board. An optical interface is used for purposes of galvanic isolation. A universal modular experiment and instrumentation SW provided by dSPACE, the so-called ControlDesk, is installed in the host PC in order to set up and control experiments. It is also used to download the model code on the DSP (DS1006 processor boards), the core of the real-time HIL simulator.

V. Experimental Results

In this section, the LIB model validation and experimental results are presented. The BMS tests performed on the HIL simulator setup comprises exemplary functional and fault insertion tests.

A. LIB Model Validation

As a first step, the electrothermal LIB model is validated in simulations. Fig. 17 shows the simulated voltage response in comparison to the real measured voltage. The dynamic load profile applied was logged in a real EV and processed for simulation. It can be noticed that the model is able to follow the measured voltage response. The same can be concluded from the temperature comparison. The starting temperature is initialized at 25 °C and stays constant due to lower dynamical driving.

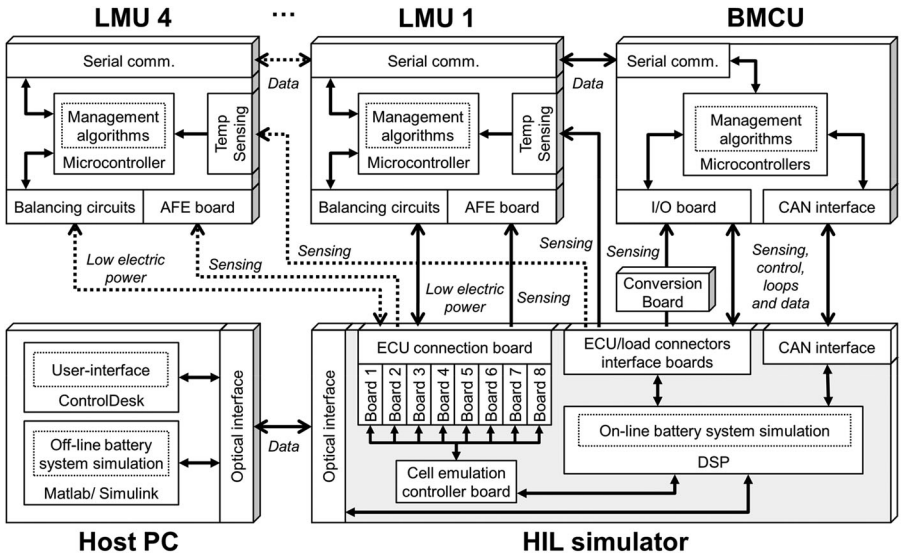

Fig. 16. Overview of main functions and interfaces between the host PC, the HIL simulator, and the BMS.

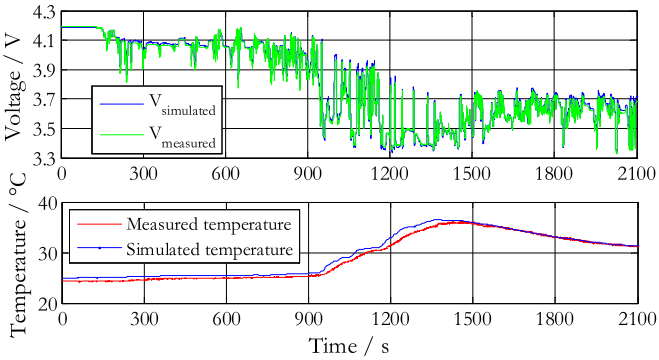

Fig. 17. Electrothermal battery model validation between measurement data and model simulation.

As soon as the load current increases, a rise in temperature is observed due to higher power losses. The model is also able to follow this trend accurately.

B. BMS Testing on HIL Simulator

In the next step, the BMS is tested on the HIL simulator running the developed system model, in the frame of functional and fault insertion testing. During functional testing, all the low-level functions of a BMS may be tested. Additionally, each of these low-level functions may be related to a particular SW and/or HW of the BMS, which, in turn, may be related to a certain electric or electronic HW interface between the BMS and the rest of the system. On the other hand, during fault insertion tests, the behavior of the system may be studied when faults are inserted either in the BMS SW or HW or its HW interfaces.

The importance of fault insertion testing lies in the ability to evaluate the reliability and robustness of a BMS, key parameters for the industry today [15], [39], [48]. Additionally, it may be of relevance to note that fault insertion testing can be classified as a form of stress testing, which, in turn, can be classified as a type of nonfunctional testing.

In this paper, only exemplary functional and fault insertion tests are presented. Although, using the same HIL simulator platform, a wider range of testing scenarios can be explored (see Table II). A comprehensive collection of functional, non-functional, and fault insertion tests will be presented in a future extension of this work. For instance, with regard to fault insertion testing, next scenarios will be considered: HW-based fault insertion in the HW interface, due to open circuit, short circuit, noise or increase of line resistance; malfunction of sensors and actuators, like temperature or current sensors; or malfunction of system-level components, like the dc-link capacitor or fuse and switch box components.

TABLE II
OVERVIEW OF FEASIBLE BMS TESTING SCENARIOS USING DEVELOPED HIL SIMULATION PLATFORM

Functional testing	Dynamic discharging.
	CC-CV charging.
	Overtemperature during discharge.
	Charging test at low temperatures.
	Overcurrent during charge.
	Short circuit(s) at cell, pack or system level.
	Overvoltage during regenerative braking.
	Diagnostic algorithms.
	Isolation monitor.
	Idle or stand-by.
	Global power consumption test.
Non-functional testing	Current, voltage, temperature accuracy.
	Baseline, compliance, endurance, load,
	Performance, recovery, scalability, stress,
	Usability and volume testing.
Fault insertion testing	Open circuit in interface(s).
	Short circuit in interface(s).
	Noise in interface(s).
	Increase of interface(s) line resistance.
	Sensor(s) malfunction.
	Actuator(s) malfunction.
	System-level component(s) malfunction.

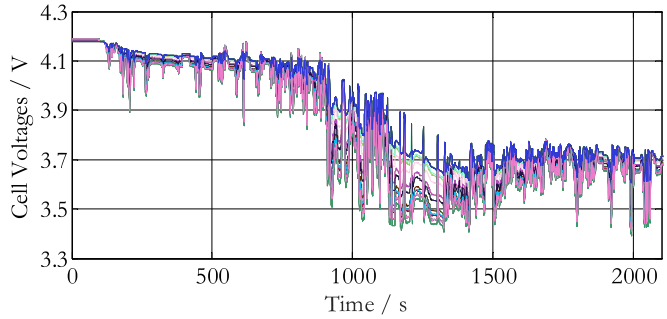

Fig. 18. HIL battery cell emulation using dynamic driving cycle.

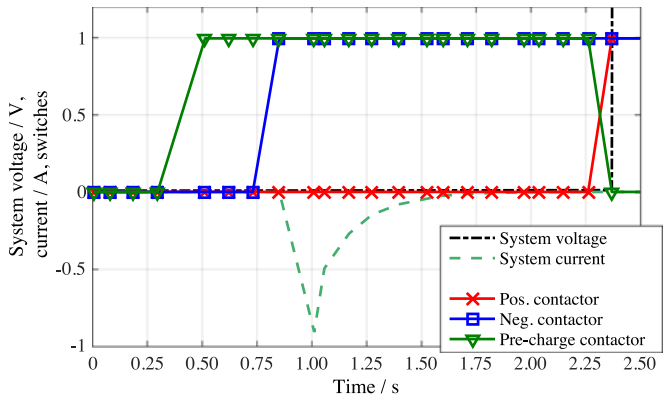

Fig. 19. Contactor logic of the BMS. Due to integration limitations, the system voltage output is only activated when contactor sequence has completed.

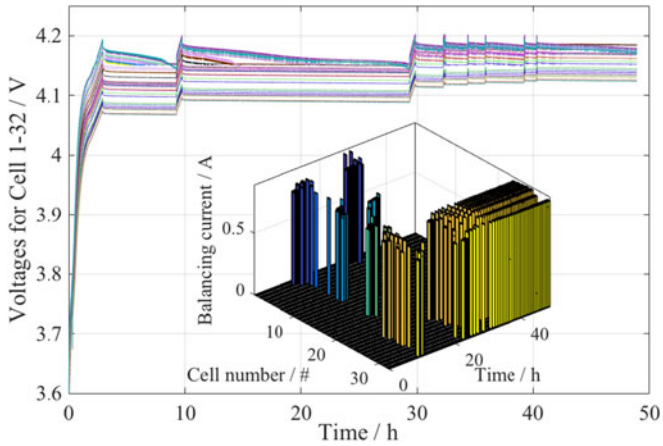

Fig. 20. CC-CV charging with balancing.

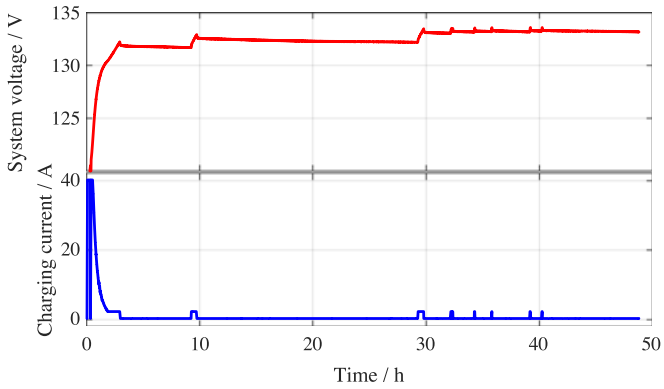

Fig. 21. System voltage and current during CC-CV charging.

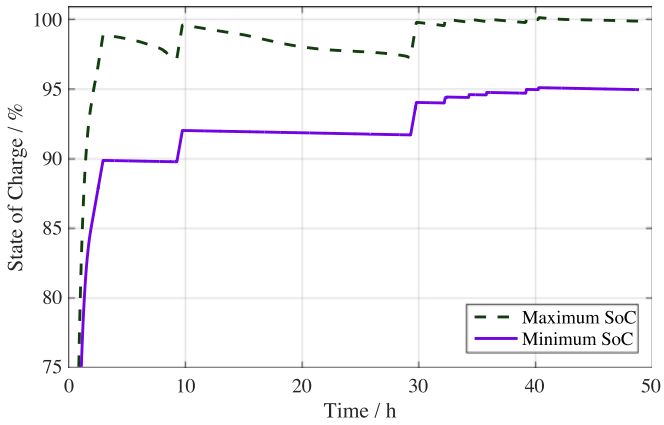

Fig. 22. Maximum and minimum cell SOC for the balancing sequence.

Last but not least, since the HIL simulator platform allows different battery pack topologies, it is also possible to test a multitude of serial, parallel, or mixed serial–parallel connections of cells. This may be important for testing battery packs consisting of multiple modules and how a BMS handles scenarios related to modules failing or being replaced.

1) Exemplary Functional Tests Results: An exemplary discharging scenario in an e-mobility application is shown in Fig. 18. Voltages of 32 cells in series during a dynamic discharge are presented. Simulation parameters such as initial cell temperature and ambient temperature are selected assuming that the underlying distribution is normal. Initial cells SOC are the result of a previous discharge/charge cycle starting from a random initial SOC distribution. Moreover, an intentionally wide random distribution of aging parameters is considered, in order to make cell-to-cell variations in capacity and impedance more marked. BMS functions related with monitoring, switch box control or protection can be checked with this functional test. With regard to the switch box control, Fig. 19 shows the contactor logic when the system operating mode changes from idle or stand-by to discharge, illustrating a precharge sequence. Note that the system voltage is not correctly modeled, but instead applied when the contactor on the positive leg of the battery pack is closed. In future work this will be added.

An exemplary CCCV charging scenario, considering gross cells SOC unbalance, is illustrated in Figs. 20–23. The same cells characteristics used for the previous discharging scenario are considered here. A random distribution of the initial SOCs of the cells within a certain window is used. The initial SOC differences are equalized by the BMS balancing circuits during the charging process, in order to maximize usable battery capacity. Note that the commercial BMS under test has a terminal voltage control algorithm for a passive balancing system implemented. The parameters for the balancing window are defined

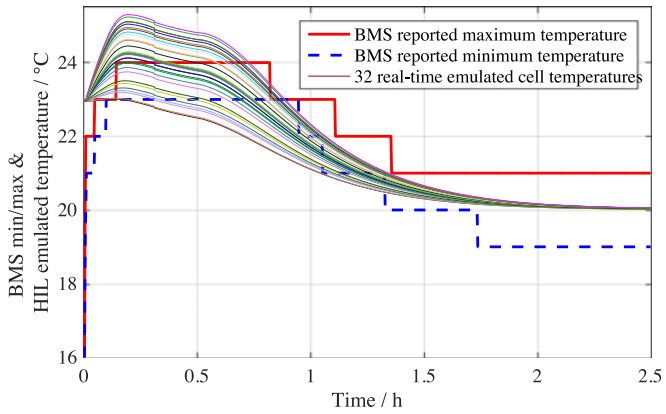

Fig. 23. Temperatures recorded during initial CC-CV charge sequence.

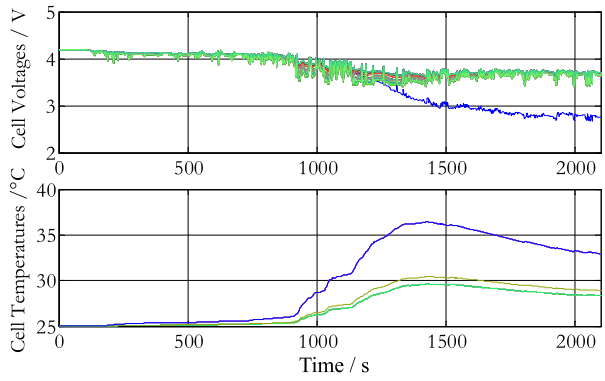

Fig. 24. Model-based fault insertion: Higher series resistance for cell 1.

in the GUI of the commercial BMS. After the BMS starts the charging process, the voltage increases gradually. As soon as the cells approach the cell target voltage window, the balancing is activated as illustrated in Fig. 20. Due to balancing, the overshoot is reduced within the allowable window. Since the value of the pack charging current is much higher than the value of the cell balancing current, at some point, the charging process has to be stopped, in order to extend time for balancing. All the cells, even though having different characteristics and initial voltages, are kept in a narrow voltage window within the cell target voltage window at the end of charge (see Figs. 20 and 21), which means that a reduced cell-to-cell variation in SOC is achieved (see Fig. 22). BMS functions such monitoring, switch box control, charge current control, balancing or protection are checked with this functional test.

2) Exemplary Fault Insertion Tests Results: Fig. 24 illustrates an exemplary failure caused by a higher internal resistance and self-discharge or cell interconnection problems. In order to emulate this fault, line resistances are added to the cell single model during operation. The figure shows the dynamic response of the system in an e-mobility application. With the aim of representing realistic operating conditions, a relatively narrow normal parameter distribution of the individual aging states is applied to the 32 cells in series of the LIB considered in the setup. At high levels of discharge or charge/regen power, the effects of this cell-to-cell parameter variation are evident. After a simulation time of 1000 s, the failure mode is

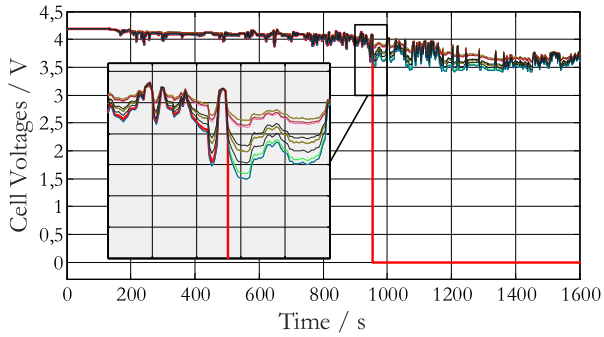

Fig. 25. Model-based fault insertion: Critical zero volt mode.

applied and within a short time the voltage of cell 1 (blue curve) tends to diverge from the average. Additionally, due to higher resistance in cell 1, the temperature is rising to a higher level in comparison to the healthy cells. Such a scenario may be detected by a BMS and counter measures may be performed, either by BMS or the energy management of the vehicle supervising unit. These measures are part of the so-called fault tolerance routines. Complex algorithms computed on a BMS master unit may be able to detect the problem. However, simpler algorithms (e.g., cell voltage average) implemented either at the master or slave level may also be able to detect the fault, providing a higher degree of redundancy. In the case of the BMS under test, fault tolerance routines against this kind of fault are not implemented. Although, the BMS under test was able to detect cell over voltage and even increase line resistance. However, the latter functionality is only effective during charging.

Another typical fault test scenario considers the interconnection error between the BMS slave board and the terminals of the cell. Loose connectors, noise, shorts, severed wires, or blown fuses may lead to erroneous voltage sensor. In Fig. 25, a critical zero volt mode is presented. Since the controller is not able to measure the cell voltage, the BMS goes into a critical fault mode. Depending on the configuration settings of the BMS controller, a further charge/discharge the pack may not be allowed. This open-circuit fault is inserted by opening a physical relay that exists in the output of the cell voltage emulation boards of the HIL simulator. Fig. 25 shows this scenario for a load driving profile with 32 cells in series. After 950 s, the cell voltage of cell 12 (red signal) suddenly drops to zero volts due to fault insertion. The same kind of test can easily be performed for the temperature sensors. However, an open circuit in temperature sensors does not lead to a critical fault mode with the BMS under test.

Another exemplary fault insertion scenario, based on an actuator malfunction, is shown in Fig. 26. In this case, a malfunction of the charging current controller is considered. Although the charging current setpoint is set to 40 A, the charger is giving 60 A, i.e., a 50 % increased current. This is easily achieved in simulation by manipulation of the control signal received from the BMS. In real life, errors in the charger or BMS settings may lead to this kind of fault. As illustrated in Fig. 26, after unsuccessful attempts to control the charger current during a few seconds, the BMS stops the charging process. A few seconds

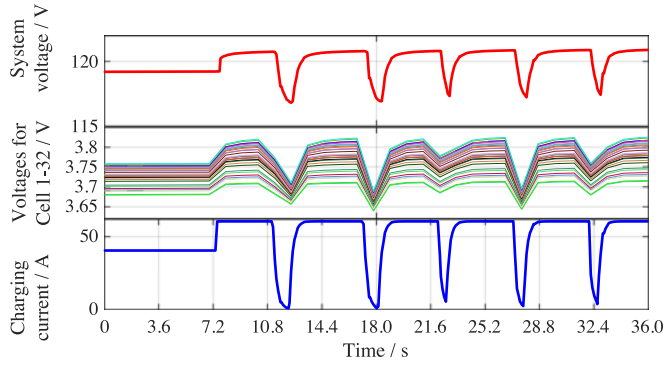

Fig. 26. System voltage, cell voltages, and system current during fault injection with 50 % increased charge current.

later, the BMS tries to start the process again, but fails again. The same cycle is repeated several times with similar results. The BMS could be configured to allow only a certain number of retries before coming into a critical fault mode.

VI. Conclusion

For purposes of general functional analysis of a BMS, simple LIB models are commonly used in HIL simulation. However, complex LIB system models are needed to ensure that all the functionalities of an advanced BMS can be analyzed and validated, including, e.g., monitoring, protection, balancing, diagnostics, or fault tolerance.

This paper presents an advanced HIL simulation battery model for testing state-of-the-art BMS on a commercial HIL simulator. In comparison with the test conducted on real batteries, BMS validation tests conducted on this platform may be more cost and time effective, easier to reproduce, and safer beyond the normal range of operation, especially at early stages in the development process or during fault simulation.

The methodology followed in this work comprises following stages:

1) comprehensive review of battery simulation approaches;
2) development of an advanced HIL simulation battery model;
3) LIB model validation in simulations;
4) BMS testing on HIL simulator, comprising exemplary functional, and fault insertion tests.

Regarding the LIB model, a nonlinear dynamic electrothermal multicell ECM coupled with an aging model is presented, taking into account temperature, aging, and SOC dependencies. Parameterization is based on experimental data from tests conducted on a commercial 40-Ah high-energy Kokam SLPB100216216H pouch cell with NMC cathode. System-level components of the battery system are also considered, like temperature sensors or the switch box.

With regard to the experimental results, first the LIB model is validated using a dynamic load profile from a real battery electric vehicle. Then, in order to prove the advanced capabilities of the HIL simulator platform, a set of exemplary functional and fault insertion tests were performed on a commercial BMS. As a final remark, a comprehensive collection of functional, nonfunctional and fault insertion tests will be presented in a future extension of this work.

Acknowledgment

The authors would like to thank The Danish Council for Strategic Research for sponsoring the following projects: the Advanced Lifetime Predictions of Battery Energy Storage and ReLiable.

References

[1] A. Ebner, F. V. Conte, and F. Pirker, "Rapid validation of battery management system with a dymola hardware-in-the-loop simulation energy storage test bench," *World Elect. Vehicle Assoc. J.*, vol. 1, pp. 205–207, 2007.

[2] Y. Yuan, X. Wei, and Z. Sun, "Assessment of power consumption control strategy for battery management system using hardware-in-the-loop simulation," in *Proc. IEEE Vehicle Power Propulsion Conf.*, 2008, pp. 1–6.

[3] Y. Li, Z. Sun, and J. Wang, "Design for battery management system hardware-in-loop test platform," in *Proc. 9th Int. Conf. Electron. Meas. Instruments*, 2009, pp. 3-339–3-402.

[4] H. Wu, "Hardware-in-loop verification of battery management system," in *Proc. 4th Int. Conf. Power Electron. Syst. Appl.*, 2011, pp. 1–3.

[5] R. Subramanian, P. Venhovens, and B. P. Keane, "Accelerated design and optimization of battery management systems using HIL simulation and rapid control prototyping," in *Proc. IEEE Int., Elect. Vehicle Conf.*, 2012, pp. 1–5.

[6] H. Rathmann, C. Weber, W. Benecke, and D. Kahler, "Sophisticated estimation of hardly measurable conditions of lithium-ion batteries," in *Proc. 39th Annu. Conf. IEEE Ind. Electron. Soc.*, 2013, pp. 1862–1866.

[7] S. Wu, Y. Zou, X. Peng, and H. Li, "Hardware-in-loop verification of battery management system with RT-LAB," in *Proc. IEEE Conf. Expo, Transp. Electrification Asia-Pacific*, 2014, pp. 1–4.

[8] Q. Wang, X. Z. Wei, and H. F. Dai, "Hardware-in-loop test platform for electric vehicle cell battery management system," *Appl. Mech. Mater.*, vol. 29–32, pp. 2398–2403, Aug. 2010.

[9] G. L. Plett, R. Billings, and M. J. Klein, "Desktop and HIL validation of hybrid-electric vehicle battery-management-system algorithms," *SAE 2007 World Congr.*, 2007.

[10] J. Zeng, J. J. Sun, and Y. Ma, "The system architecture design about test platform of battery management system," *Adv. Mater. Res.*, vol. 645, pp. 217–220, Jan. 2013.

[11] A. Collet, J. Crebier, and A. Chureau, "Multi-cell battery emulator for advanced battery management system benchmarking," in *Proc. IEEE Int. Symp. Ind. Electron.*, 2011, pp. 1093–1099.

[12] H. Dai, X. Zhang, X. Wei, Z. Sun, J. Wang, and F. Hu, "Cell-BMS validation with a hardware-in-the-loop simulation of lithium-ion battery cells for electric vehicles," *Int. J. Electr. Power Energy Syst.*, vol. 52, pp. 174–184, Nov. 2013.

[13] W. C. Lee and D. Drury, "Development of a hardware-in-the-loop simulation system for testing cell balancing circuits," *IEEE Trans., Power Electron.*, vol. 28, no. 12, pp. 5949–5959, Dec. 2013.

[14] J. V. Barreras, C. Pinto, R. de Castro, E. Schaltz, S. J. Andreasen, and R. E. Araujo, "Multi-objective control of balancing systems for Li-ion battery packs: A paradigm shift?" in *Proc. IEEE Vehicle Power Propulsion Conf.*, 2014, pp. 1–7.

[15] W. Waag, C. Fleischer, and D. U. Sauer, "Critical review of the methods for monitoring of lithium-ion batteries in electric and hybrid vehicles," *J. Power Sources*, vol. 258, pp. 321–339, 2014.

[16] M. Einhorn, W. Roessler, and J. Fleig, "Improved performance of serially connected li-ion batteries with active cell balancing in electric vehicles," *IEEE Trans. Veh. Technol.*, vol. 60, no. 6, pp. 2448–2457, Jul. 2011.

[17] S. Buller, *Impedance Based Simulation Models for Energy Storage Devices in Advanced Automotive Power Systems* (Aachener Beiträge des ISEA). Maastricht, Germany: Shaker Verlag GmbH, 2003.

[18] D. Andre, M. Meiler, K. Steiner, H. Walz, T. Soczka-Guth, and D. U. Sauer, "Characterization of high-power lithium-ion batteries by electrochemical impedance spectroscopy. II: Modelling," *J. Power Sources*, vol. 196, no. 12, pp. 5349–5356, Jun. 2011.

[19] D. Andre, M. Meiler, K. Steiner, C. Wimmer, T. Soczka-Guth, and D. U. Sauer, "Characterization of high-power lithium-ion batteries by electrochemical impedance spectroscopy. I. Experimental investigation," *J. Power Sources*, vol. 196, no. 12, pp. 5334–5341, Jun. 2011.

[20] N. Shidore *et al.*, "Battery in the loop: Battery evaluation in a systems context," in *Proc. IEEE Trans. Electrification Conf. Expo.*, 2014, pp. 1–9.
[21] H.-S. Song *et al.*, "Verification of battery system model for environmentally friendly vehicles using a battery hardware-in-the-loop simulation," *IET Power Electron.*, vol. 6, no. 2, pp. 417–424, Feb. 2013.
[22] S. Kermani, R. Trigui, S. Delprat, B. Jeanneret, and T. M. Guerra, "PHIL Implementation of energy management optimization for a parallel HEV on a predefined route," *IEEE Trans. Veh. Technol.*, vol. 60, no. 3, pp. 782–792, Mar. 2011.
[23] Y. Xiao-kun, H. Hong-wen, P. Lian-yun, and Z. Xiaolin, "Hardware-in-the-loop simulation on a hybrid power system," in *Proc. 4th Int. Conf. Power Electron. Syst. Appl.*, 2011, pp. 1–5.
[24] C. Seitl, J. Kathan, G. Lauss, and F. Lehfuss, "Power hardware-in-the-loop implementation and verification of a real time capable battery model," in *Proc. IEEE 23rd Int. Symp. Ind. Electron.*, 2014, pp. 2285–2290.
[25] T. Mesbahi, N. Rizoug, P. Bartholomeus, and P. Le Moigne, "Li-ion battery emulator for electric vehicle applications," in *Proc. IEEE Vehicle Power Propulsion Conf.*, 2013, pp. 1–8.
[26] O. Konig, C. Hametner, G. Prochart, and S. Jakubek, "Battery emulation for power-HIL using local model networks and robust impedance control," *IEEE Trans. Ind. Electron.*, vol. 61, no. 2, pp. 943–955, Feb. 2014.
[27] A. Thanheiser, W. Meyer, D. Buecherl, and H. Herzog, "Design and investigation of a modular battery simulator system," in *Proc. IEEE Vehicle Power Propulsion Conf.*, 2009, pp. 1525–1528.
[28] O. Konig, S. Jakubek, and G. Prochart, "Battery impedance emulation for hybrid and electric powertrain testing," in *Proc. IEEE Vehicle Power Propulsion Conf.*, 2012, pp. 627–632.
[29] G. Pebriyanti, "A lithium-ion battery modeling for a HIL-battery simulator," in *Proc. Int. Conf. Comput., Control, Informat. Appl.*, 2013, pp. 185–190.
[30] L. f. Xu, J. q. Li, J. f. Hua, X. j. Li, and M. g. Ouyang, "Hardware in the loop simulation of vehicle controller unit for fuel cell/battery hybrid bus," in *Proc. IEEE Vehicle Power Propulsion Conf.*, 2009, pp. 1777–1782.
[31] C. Park, J. Liu, and P. H. Chou, "B#: A battery emulator and power-profiling instrument," in *Proc. Int. Symp. Low Power Electron. Des.*, 2003, pp. 288–293.
[32] A. Florescu, S. Bacha, A. Rumeau, I. Munteanu, and A. I. Bratcu, "PHIL simulation for validating power management strategies in all-electric vehicles," in *Proc. 15th Eur. Conf. Power Electron. Appl.*, 2013, pp. 1–6.
[33] A. Rousseau *et al.*, "Electric drive vehicle development and evaluation using system simulation," in *Proc. 19th IFAC World Congr.*, 2014, pp. 7886–7891.
[34] A. Thanheiser, T. P. Kohler, C. Bertram, and H. Herzog, "Battery emulation considering thermal behavior," in *Proc. IEEE Vehicle Power Propulsion Conf.*, 2011, pp. 1–5.
[35] T. Baumhofer, W. Waag, and D. U. Sauer, "Specialized battery emulator for automotive electrical systems," in *Proc. IEEE Vehicle Power Propulsion Conf.*, 2010, pp. 1–4.
[36] D. Bazargan and S. Filizadeh, "Hardware-in-loop real-time simulation of a battery storage system in a wind generation scheme," in *Proc. 3rd Int. Conf. Elect. Power Energy Convers. Syst.*, 2013, pp. 1–6.
[37] D. Kawashima, M. Ihara, T. Shen, and H. Nishi, "Real-time simulation of cooperative demand control method with batteries," in *Proc. 38th Annu. Conf. IEEE Ind. Electron. Soc.*, 2012, pp. 3588–3593.
[38] W. W. Weaver and G. G. Parker, "Real-time hardware-in-the-loop simulation for optimal dc microgrid control development," in *Proc. IEEE 15th Workshop Control Model. Power Electron.*, 2014, pp. 1–6.
[39] H. Rahimi-Eichi, U. Ojha, F. Baronti, and M. Y. Chow, "Battery management system: An overview of its application in the smart grid and electric vehicles," *IEEE Ind. Electron. Mag.*, vol. 7, no. 2, pp. 4–16, Jun. 2013.
[40] L. Gao, S. Liu, and R. A. Dougal, "Dynamic lithium-ion battery model for system simulation," *IEEE Trans. Compon. Packag. Technol.*, vol. 25, no. 3, pp. 495–505, Sep. 2002.
[41] M. Chen and G. A. Rincon-Mora, "Accurate electrical battery model capable of predicting runtime and i-v performance," *IEEE Trans. Energy Convers.*, vol. 21, no. 2, pp. 504–511, Jun. 2006.
[42] M. A. Roscher and D. U. Sauer, "Dynamic electric behavior and open-circuit-voltage modeling of LiFePo4-based lithium ion secondary batteries," *J. Power Sources*, vol. 196, no. 1, pp. 331–336, 2011.
[43] J. V. Barreras, E. Schaltz, S. J. Andreasen, and T. Minko, "Datasheet-based modeling of li-ion batteries," in *Proc. IEEE Vehicle Power Propulsion Conf.*, Oct. 2012, pp. 830–835.
[44] W. F. Bentley, "Cell balancing considerations for lithium-ion battery systems," in *Proc. 12th Annu. Battery Conf. Appl. Adv.*, Jan. 1997, pp. 223–226.
[45] "Comparison and evaluation of charge equalization technique for series connected batteries," in *Proc. IEEE 37th Power Electron., Specialists Conf.*, Jun. 2006, pp. 1–6.
[46] J. Cao, N. Schofield, and A. Emadi, "Battery balancing methods: A comprehensive review," in *Proc. IEEE Vehicle Power Propulsion Conf.*, Sep. 2008, pp. 1–6.
[47] A. A. Pesaran, "Battery thermal models for hybrid vehicle simulations," *J. Power Sources*, vol. 110, no. 2, pp. 377–382, 2002.
[48] S. Abada, G. Marlair, A. Lecocq, M. Petit, V. Sauvant-Moynot, and F. Huet, "Safety focused modeling of lithium-ion batteries: A review," *J. Power Sources*, vol. 306, pp. 178–192, 2016.
[49] T. Veijola, "Electrothermal simulation models for NTC and PTC thermistors," *Proc. CSC*, vol. 2, pp. 950–955, 1998.
[50] D. Stanković and M. Zlatanović, "A versatile computer controlled measuring system for recording voltage-current characteristics of various resistance sensors," *Sens. Actuators A, Phys.*, vol. 42, no. 1, pp. 612–616, 1994.

Jorge Varela Barreras was born in Vigo, Spain, in 1982. He received the M.Sc. degree in industrial engineering from the University of Vigo, Vigo, Spain, and the M.Sc. degree in enery engineering and the Ph.D. degree in battery management from Aalborg University, Aalborg, Denmark, in 2009 and 2016, respectively.

In 2010, he co-founded a photovoltaic consulting company in Spain, serving as a Business Development Manager. Since 2011, he has been a Researcher in Aalborg. In June 2016, he became a Postdoctoral Researcher at the University of Oxford, Oxford, U.K. His research interests include novel electric vehicle concepts and Li-ion battery modeling, simulation, emulation, diagnostics, balancing and management systems.

Christian Fleischer studied M.Sc. degree in electrical and computer engineering with a focus on statistical signal processing and high performance computing from Ohio State University, Columbus, OH, USA, in 2009. He is currently working toward the Ph.D. degree at Rheinisch - Westfälische Technische Hochschule (RWTH) Aachen University, Aachen, Germany.

Since 2009, he has been working as a Research Scientist at the Institute of Power Electronics and Electrical Drives in the Electrochemical Energy Conversion and Storage Systems Group. His research interests include integration of battery management systems, specializing on developing novel adaptive on-line state and parameter estimation methods based on probabilistic inference and machine learning algorithms, creation of the software architecture, and integration of AUTOSAR components.

Andreas Elkjær Christensen received the M.Sc. degree in engineering from the Technical University of Denmark, Lyngby, Denmark, in 2009, and the industrial Ph.D. degree, which was a collaboration between Lithium Balance A/S, Denmark, and DTU Energy, from the Technical University of Denmark in 2016.

During his Ph.D., he researched new battery technology in form of Lithium-air batteries, with special focus on applications of electrochemical impedance spectroscopy for battery management. This work has resulted in two pending patents. His work at Lithium Balance A/S is focused on project management, embedded software development, functional safety in road vehicles, and supervising patent applications and grants.

Dr. Christensen is a Board Member at the Danish Battery Society.

Maciej Swierczynski received the B.Tech. degree in computer engineering for industrial applications from AGH University of Science and Technology, Krakow, Poland, in 2005; the M.Tech degree in computer engineering for industrial applications and in power electronics and drives from Aalborg University, Aalborg, Denmark, in 2007 and 2009, respectively; and the Ph.D. degree with a thesis on Lithium-ion battery energy storage system for augmented wind power plants from Aalborg University.

He is working currently as an Associate Professor with Aalborg University. His research interests include energy storage technologies for wind and automotive applications, battery testing, modeling, and lifetime analyses.

Erik Schaltz was born in Viborg, Denmark, in 1981. He received the M.Sc. and Ph.D. degrees in electrical engineering from the Department of Energy Technology, Aalborg University, Aalborg, Denmark, in 2005 and 2010, respectively.

From 2009 to 2012, he was an Assistant Professor in the Department of Energy Technology, Aalborg University, where he is currently an Associate Professor and the Programme Leader of the research programme in E-mobility and Industrial Drives. His research interests include analysis, modeling, design, and control of power electronics; electric machines; energy storage devices including batteries and ultracapacitors; fuel cells; hybrid electric vehicles; thermoelectric generators; and inductive power transfer systems.

Søren Juhl Andreasen was born in Aalborg, Denmark, in 1981. He received the M.Sc.M.E. degree with specialization in electromechanical system design, and the Ph.D. degree in design and control of high temperature proton exchange membrane fuel cell system from Aalborg University, Aalborg, Denmark, in 2005 and 2009, respectively.

Since 2014, he has been working as a Senior System Engineer with the Development Department at Serenergy A/S. His work includes research and development related to methanol reformer and high temperature PEM fuel cell systems. Products include uninterruptible power supply, auxiliary power unit, and hybrid electric systems for mobile power. In 2012, he worked as an Associate Professor at Aalborg University. His involvements in research concerned fuel cell and battery power systems.

Dirk Uwe Sauer received the Dr.-rer.-nat. degree from the Faculty of Natural Sciences, University of Ulm, Ulm, Germany, in 2003.

He is currently the Head of the Group for Electrochemical Energy Conversion and Storage Systems with Rheinisch - Westfälische Technische Hochschule (RWTH) Aachen University, Aachen, Germany. In 2003, he was appointed as a Junior Professor and in 2009 he became a Full Professor. Beforehand, he worked for nine years at the Fraunhofer Institute for Solar Energy Systems, Freiburg, Germany. His focus is on the integration of renewable energies into grids with the support of energy storage systems and on batteries for electromobility. He is also a Co-founder of the companies P3 Energy Storage GmbH, BatterieIngenieure GmbH, and eBusplan GmbH.